Joule

CellPress

Article

Vacuum insulation arrays as damage-resilient thermal superinsulation materials for energy saving

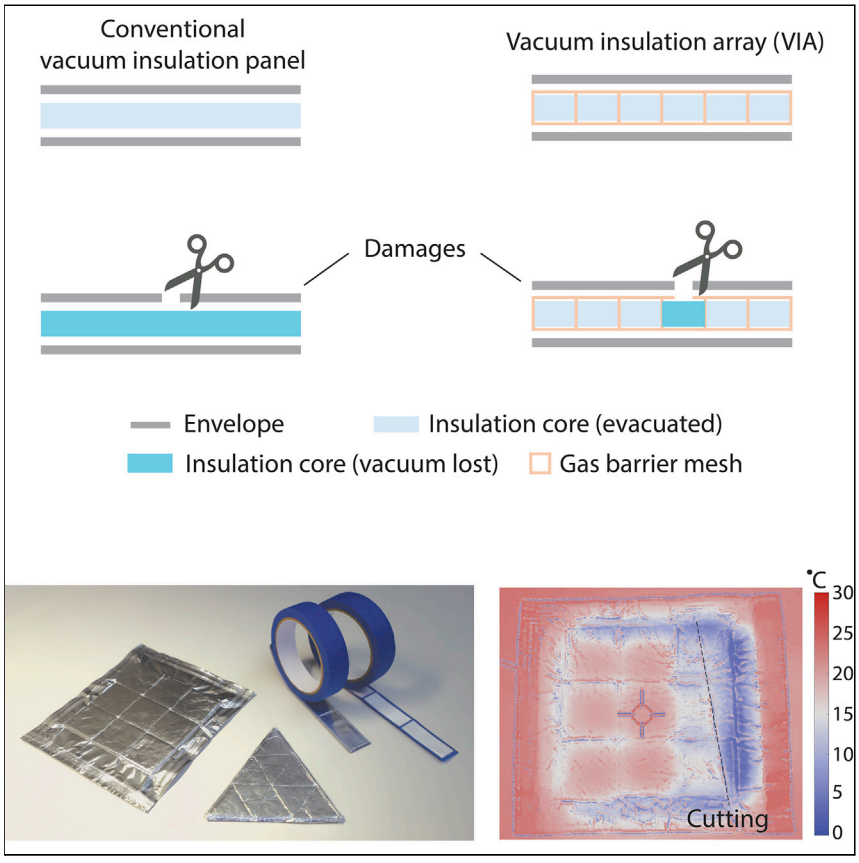

The building sector makes a significant contribution to the global greenhouse gas emission, where space heating and cooling is the dominant culprit. While it is well known that significant energy can be saved by thermally insulating buildings, the current insulation materials either do not have sufficient insulation performance (e.g., foam and fiberglass mat) or are often mechanically vulnerable to forces and damage (e.g., aerogels and vacuum insulation panels). We design and demonstrate a thermal superinsulation material that combines ultralow thermal conductivity and mechanical robustness. This design provides flexibility and adaptability similar to those in conventional insulation materials while offering insulation performance on par with the best insulation materials.

Jiawei Zhou, Yucan Peng, Jinwei Xu, Yecun Wu, Zhuojun Huang, Xin Xiao, Yi Cui

yicui@stanford.edu

Highlights

Vacuum insulation array design achieves ultrahigh insulation performance

Hermetic sealing with gas-barrier materials ensures that damage is limited to local areas

Puncture, cutting, and reassembly are allowed with insulation performance being maintained

Zhou et al., Joule 6, 2358–2371
October 19, 2022
https://doi.org/10.1016/j.joule.2022.07.015

CellPress

Joule

Article

Vacuum insulation arrays as damage-resilient thermal superinsulation materials for energy saving

Jiawei Zhou,[1] Yucan Peng,[1] Jinwei Xu,[1] Yecun Wu,[2] Zhuojun Huang,[1] Xin Xiao,[1] and Yi Cui[1,3,4,*]

SUMMARY

The building sector, where heating and cooling are the major energy consumers, contributes significantly to global greenhouse gas emissions. Large energy savings can be achieved if buildings are thermally insulated from the environment. Existing high-thermal insulation materials, such as aerogels and vacuum insulation panels, are vulnerable to mechanical forces and damage, making their installation a significant challenge and compromising their long-term performance. Here, we report a vacuum insulation array (VIA) design that combines mechanical robustness and ultrahigh thermal-insulation performance, with local vacuum cells that are hermetically sealed and separated from each other. This design allows the material to be punctured, cut, or reassembled, with a long-term thermal conductivity of less than 0.007 W/m-K even after puncture damage. Our insulation material can potentially realize a 20%–40% reduction in the annual energy use for the existing building-space heating and cooling with only 2 cm of added thickness.

INTRODUCTION

Heating and cooling needs comprise a large portion of our society's total energy consumption. In the building sector alone, heating and cooling account for over 30% of global building energy end use[1] and are responsible for about 4 Gt of CO_2 emission, including both direct and indirect contributions,[2] which continues to increase due to global urbanization. Likewise, in the transportation area, cold-chain transport and storage of commodities including food, medicine, and even liquefied fuels demand increasing cooling capacity. A dominant culprit of energy consumption is the heat exchange with the environment. For example, in the building sector, a well-designed building thermal envelope can lead to significant energy saving and potentially realize buildings with net-zero energy consumptions,[3] as highlighted by the "Passive House" standard.[4]

Windows, walls, and roofs are among the most important components of the building thermal envelope. Significant efforts in recent years have been devoted to developing energy-efficient windows, with examples including electrochromic or thermochromic dynamic windows,[5–7] photovoltaic windows,[8,9] aerogel-based window glazing,[10] and flexible low-emissivity films for retrofit.[11] Passive radiative cooling[12–15] and season-dependent radiative designs[16] have also emerged to reduce building energy consumption by regulating both solar absorption and thermal emission at the same time. An even greater energy-saving potential exists in transforming the walls and roofs into thermal superinsulation structures, which will significantly reduce the heat exchange between the building and the environment.[17] A desired thermal-insulation material used for walls

CONTEXT & SCALE

Energy spent on heating and cooling makes up the largest share of the end energy use in the building sector, which in turn contributes to nearly one-third of the global greenhouse gas emissions. To cut down the emissions in the building sector, an effective way is to improve the thermal insulation of buildings. Compared with conventional foam and loose-fill-type insulation materials, high-performance materials, e.g., aerogels and vacuum insulation panels, provide superior thermal-insulation performance. However, these materials are vulnerable to damage, making their installation a challenging task. We design a thermal superinsulation material that possesses both high insulation performance and installation convenience. We create local vacuum insulations that are hermetically separated from each other by gas barriers. This design allows the material to be cut and reassembled like conventional foam insulations while maintaining a high insulation performance comparable with the best vacuum insulation panels.

and roofs should have a long-term insulation performance of at least 20 R/in (an equivalent thermal conductivity of about 0.007 W/m-K) to minimize the thickness needed.[17] Conventional insulation materials, such as fiberglass mat, cellulosic fibers, and polymeric foams, cannot meet this target due to the gaseous heat conduction of air within the pores, contributing to total thermal conductivities often higher than 0.03 W/m-K.[18,19] Synthesized nanomaterials, such as aerogels, can achieve thermal conductivity in the range of 0.01–0.02 W/m-K,[20–27] with the lowest reaching about 9 mW/m-K in silica aerogel at ambient pressure.[26] However, aerogels are often mechanically fragile and have high manufacturing costs, and their insulating properties still fall short of the desired insulation performance.

For porous insulation materials, gaseous heat conduction of air (0.026 W/m-K for air at standard conditions) makes a significant contribution to the total thermal conductivity.[28] By evacuating the air out, gaseous heat conduction can be greatly suppressed when air mean free path becomes larger than the pore size.[29] Vacuum insulation panel exploits this effect by sealing a porous core material under vacuum with a gas-barrier envelope.[30–32] Owing to the evacuation of air, their thermal-insulation performance significantly outpaces conventional insulation materials, achieving thermal conductivity as low as 0.003–0.008 W/m-K. However, a major challenge limiting their adoption is that these panels cannot be cut on site and extreme care has to be taken during handling,[33] because any damage on the panel would lead to a vacuum loss and consequently a large degradation in the insulation performance. This makes them less adaptable to various practical applications.

In this work, we design and demonstrate a superinsulation material that combines the ultrahigh thermal-insulation performance (i.e., long-term thermal conductivity of less than 0.007 W/m-K) and the installation convenience of conventional insulation materials. Conventional vacuum insulation panels are vulnerable to damage as the vacuum is protected by only one envelope (Figure 1A). The key to our design is a hermetically sealed structure that separates the inner volume into an array of vacuum cells, each protected by an individual gas-barrier film (Figure 1B), which is sealed together with the envelope. For our design, the vacuum loss caused by any damage will be limited to a local area, and the major portion of the material remains under vacuum. As a result, the material can be cut and reassembled without losing its overall insulation performance. This vacuum insulation array (VIA) design provides the flexibility and adaptability required for practical applications and can be made into different product configurations (panels, tapes, etc., Figure 1C), while offering significantly better insulating performance compared with conventional insulation materials (Figure 1D).

RESULTS

Design and fabrication of vacuum insulation array

The physical properties of the gas-barrier material are critical to the long-term thermal-insulation performance of VIA. First, the introduced gas-barrier structure conducts heat, and materials with low thermal conductivities are desired. Second, when local damage occurs, the gas-barrier material needs to block the air from infiltrating into adjacent cells, thus requiring materials with low gas permeation rates. Our thermal modeling shows that the gas-barrier material needs to have a thermal conductivity less than 0.3 W/m-K for cell sizes smaller than 5 × 5 cm^2, in order to achieve a total thermal conductivity lower than 0.006 W/m-K (Figure 2A). Figure 2B compares the oxygen permeability of different materials as a quantification of the gas-barrier performance[34–36] along with their thermal conductivities. Based on the two criteria, we have chosen nylon and ethylene vinyl alcohol (EVOH) as the major

[1]Department of Materials Science and Engineering, Stanford University, Stanford, CA 94305, USA

[2]Department of Electrical Engineering, Stanford University, Stanford, CA 94305, USA

[3]Stanford Institute for Materials and Energy Sciences, SLAC National Accelerator Laboratory, Menlo Park, CA 94025, USA

[4]Lead contact

*Correspondence: yicui@stanford.edu

https://doi.org/10.1016/j.joule.2022.07.015

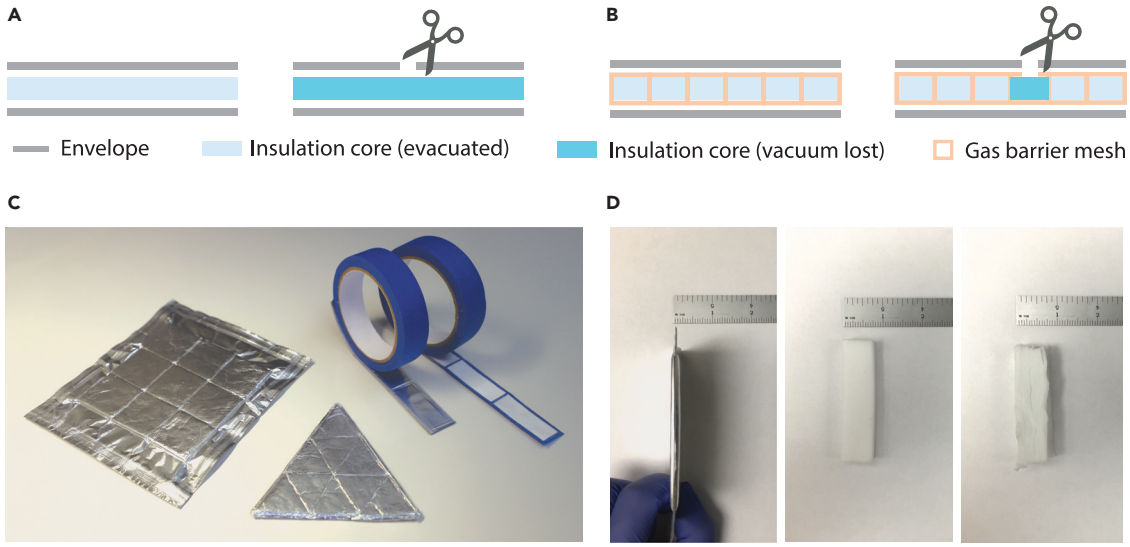

Figure 1. Conventional vacuum insulation and our design

(A) Conventional vacuum insulation panel is protected by only one envelope layer. Any damage in the envelope leads to vacuum loss.

(B) Our vacuum insulation array incorporates a gas-barrier mesh that separates the core material into individual cells such that damage only leads to local vacuum loss.

(C) The concept of vacuum insulation array can be applied to different product configurations, such as panels or tapes.

(D) Comparison of thickness for different insulation materials with the same insulation performance. Left to right: vacuum insulation, foam, and fiberglass mat.

components of the gas-barrier film, owing to their simultaneously low thermal conductivity and low oxygen permeability. We have quantified the gas-barrier performance of nylon and EVOH barrier films by studying the thermal-conductivity variation with time for vacuum insulation materials sealed using these films as envelope on one side (see inset of Figure 2C for illustration of measurement configuration). Polyethylene (PE) films are also tested as a comparison. For these tests, significant gas leakage through the polymer barrier films would occur, allowing us to observe thermal-conductivity changes within a reasonable time frame. With PE films as the envelope, the thermal conductivity rapidly rises to above 0.006 W/m-K within about 2 h, since air permeates PE relatively easily. In contrast, the thermal conductivity remains below 0.006 W/m-K for about 2 weeks for nylon barrier films and for EVOH barrier film stays so for nearly a month (Figure 2C). These thermal-conductivity changes are also consistent with the gas permeation rates for nylon and EVOH barrier films (see supplemental information).

To fabricate this vacuum array structure, it is crucial to ensure a hermetic seal between the envelope and the gas-barrier structure. We start with a laminated gas-barrier film containing a thin sealing layer on one side (Figure 2D). The sealing layers are usually made of thermoplastic polymers whose interdiffusion at higher temperatures can create strong bonds. (In our case the sealing layer is PE, which is one of the most common polymers used as sealing layers in the packaging industry.[34]) Porous core materials are first covered by the gas-barrier film with the sealing layer facing outward, which are then enclosed by envelope films. The envelope film also has a sealing layer on the inner side which has to be compatible with the sealing layer of the gas-barrier film. Next, air is evacuated from the structure and the envelopes are sealed together under vacuum. Lastly, the entire structure is pressed between hot plates at a temperature slightly above the melting point of the sealing layer for a short duration. The interdiffusion of PE bonds the layers together. After cooling,

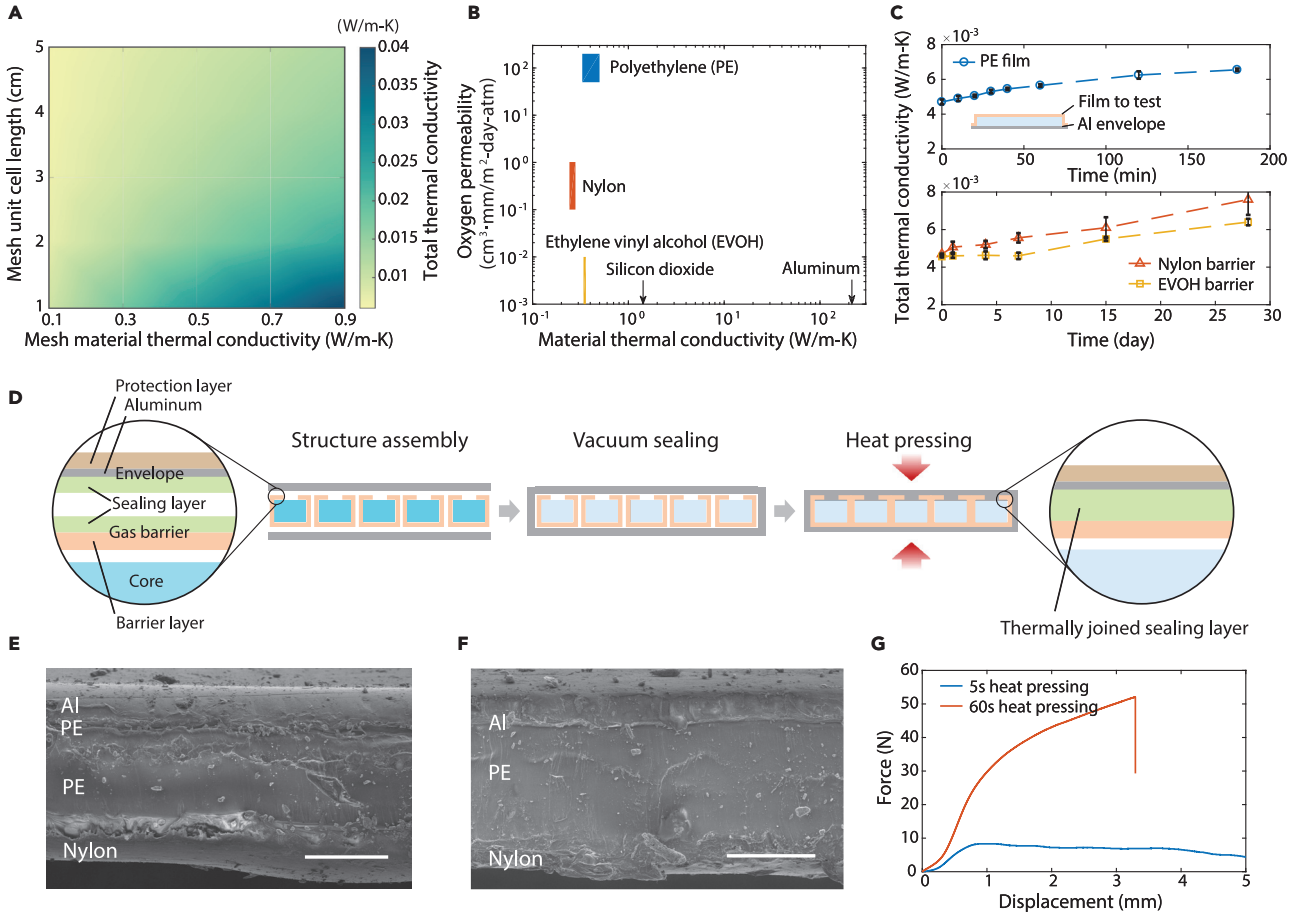

Figure 2. Design and fabrication of VIA

(A) Thermal-conductivity modeling of the vacuum insulation array. The maximum unit cell dimension is limited to 5 cm because such a cell size would be a small fraction of a practical insulation panel typically having an area on the order of 1 m^2. The total thermal conductivity, including the gas-barrier structure, is shown as colors.

(B) Material selection for the gas-barrier structure based on oxygen permeability and thermal conductivity.

(C) Gas permeation rate measurement for different gas-barrier films. The size of the sealed vacuum insulation is 6.5 × 7.5 × 0.33 cm^3. The error bars are the standard deviations of the measurement results averaged over at least three samples.

(D) Schematic of the manufacturing process, including structure assembly, vacuum sealing, and heat pressing. The sealing between the envelope and gas-barrier structure is achieved by the thermal bonding of the sealing layers.

(E and F) Cross-sectional SEM images of the sealed region for 5 s sealing time (E) and 60 s sealing time (F). Scale bars: 100 μm.

(G) Mechanical peeling test of the bonding between envelope and gas-barrier film.

the gas barrier and envelopes are sealed together by the thermally joined sealing layer (Figure 2D). Figures 2E and 2F show the cross-sectional scanning electron microscopy images of the sealed region after heat-pressing steps for different pressing durations. For 5 s of heat pressing, the interdiffusion of PE is not sufficient, and boundaries can be clearly seen (Figure 2E). When the duration is increased to 1 min, two sealing layers have joined together without apparent boundaries (Figure 2F). Other heat-pressing durations have also been tried (Figure S1). In general, for duration longer than 30 s most regions show good sealing results. We also note that excess heat pressing in general is not an issue for the VIA structure, because the core materials (e.g., fumed silica and fiberglass) usually can withstand much higher temperatures. However, it is preferable to avoid excess heat pressing because at higher temperatures additional gas leakages may happen through the sealing regions between the envelopes. We have found that limiting the heat-pressing

duration to less than 5 min introduces negligible effects on the VIA structure. For all later results, we have chosen 1 min for the heat-pressing step to ensure that good sealing is achieved between the gas-barrier films and aluminum envelopes. The successful thermal bonding is also confirmed by a mechanical peeling test (Figure 2G). With longer duration, the mechanical peeling breakage happens within the envelope film. The strong bonding between the envelope and the gas-barrier films ensures a hermetically sealed VIA structure.

Thermal-insulation and damage-resilience performances

We characterized the thermal-insulation performance of VIA and its resilience to damage using a home-built thermal-conductivity measurement setup based on the heat flowmeter method (see experimental procedures; Figure S2). The limited area of the heat flux sensor allows probing thermal conductivity at different locations. While larger cell dimensions can lead to a lower overall thermal conductivity (Figure S3), we have fixed the cell size to be 3.8 × 3.8 cm^2 for consistent discussions. Figures 3A and 3B shows the measured thermal conductivity at different spots on a three-by-three square VIA. When the material is intact, the thermal conductivity is about 0.005–0.006 W/m-K (Figure 3A). After one corner cell is punctured, only the damaged area shows significantly increased thermal conductivity, and other areas remain unaffected (Figure 3B). We also performed a similar test by cutting off one column of cells from a square VIA. Regions that are not directly affected by cutting remain at low thermal conductivities (Figure 3C).

While the heat flowmeter method allows probing the thermal-conductivity changes locally, the practical insulation performance will depend on the overall thermal conductivity over a larger area. We measured an average thermal conductivity over an area of 10.2 × 10.2 cm^2 to be 0.0092 W/m-K using a guarded hot plate setup (Figure S4). This value is higher than the thermal modeling result mainly because of the edge heat conduction due to the limited size of our three-by-three VIA (Figure S5A). Nonetheless, one could stack two VIAs on top of each other with their cell arrays mismatched to minimize the edge heat conduction (Figure S5B). The average thermal conductivity of such stacked VIA is 0.0062 W/m-K. Such stacking could be effective in practical applications to minimize the thermal-bridging effects. Nevertheless, for later discussions the thermal conductivities are obtained using the heat flowmeter method for one VIA layer only unless otherwise specified, as we focus on the resilience of VIA to local damage.

An important requirement for effective vacuum insulation is the ability to maintain a vacuum for a long term, even when damage occurs. Figure 3D shows the thermal conductivity at the center of a three-by-three square VIA after a corner cell is punctured. When nylon is used as the gas-barrier material, the thermal conductivity remains below 0.006 W/m-K for 1 month, and only shows a slight increase after 2 months. In comparison, the VIA with an EVOH barrier film has no apparent change in the thermal conductivity for up to 2 months. We further measured the thermal conductivity of these samples after 1 year. While the VIA with nylon gas barrier shows higher thermal conductivity, The VIA with EVOH maintains a low thermal conductivity of about 0.007 W/m-K (Figure 3D). This demonstrates the ability of the VIA design to maintain a high thermal-insulation performance even with damage for a long period. Moreover, we note that the gas permeation after local vacuum loss is a sequential process—the air goes through adjacent cells first and then penetrates cells further away. The array geometry can thus help to maintain the high thermal-insulation performance for a long period even after damage (see experimental procedures; Figure S6). The thermal-conductivity measurement for the VIA with a nylon barrier with a corner cell damaged after

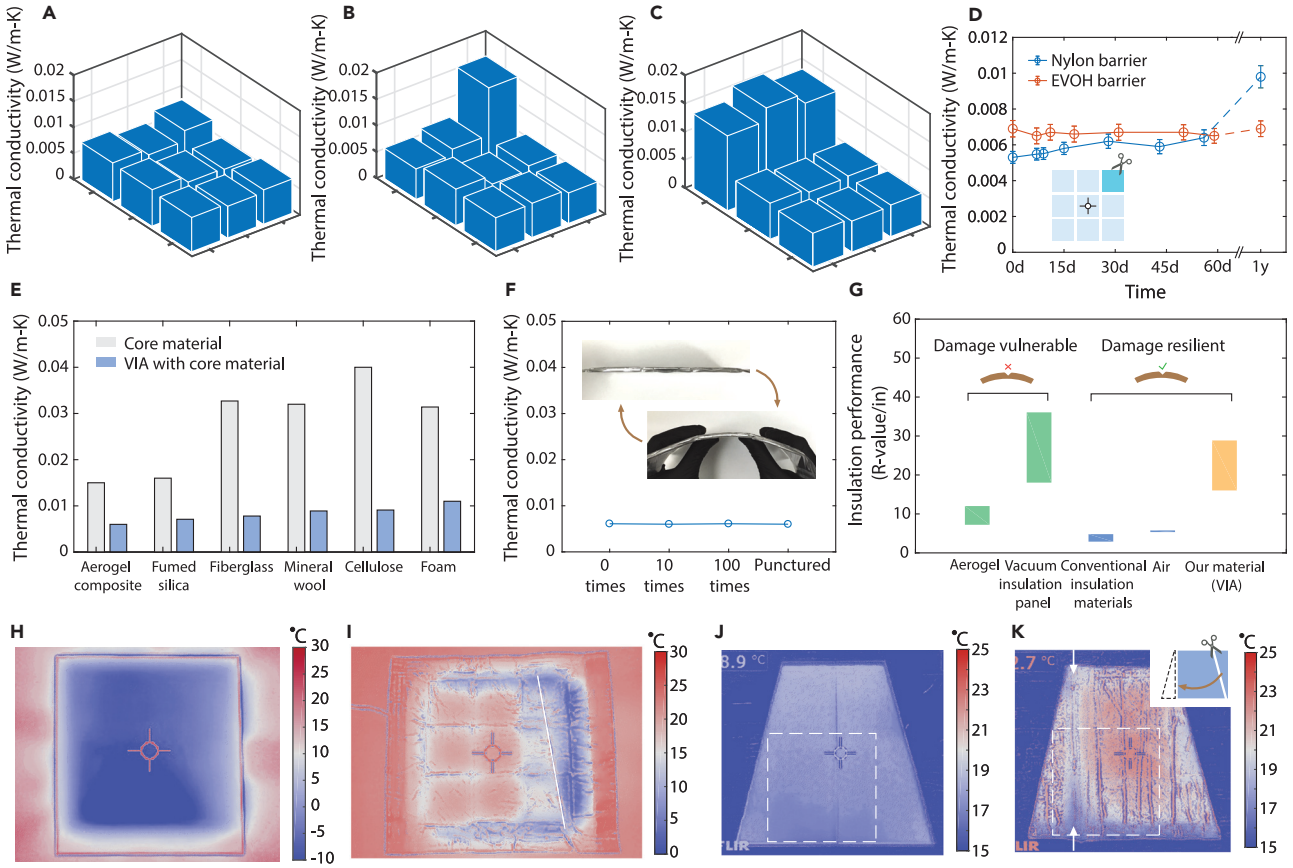

Figure 3. Thermal-insulation and damage-resilience performances of VIA

(A–C) Thermal conductivities at different locations for a three-by-three square VIA, before any damage (A), after a puncture damage at one corner cell (B), and after cutting along one column of cells (C). The cell dimension is 3.8 × 3.8 cm^2.

(D) Thermal conductivity of the central cell of a three-by-three square VIA after one corner cell is damaged. The higher initial thermal conductivity with EVOH barrier compared with nylon is likely to come from the out-gassing of certain organics used in the laminate film during the heat-pressing step. The error bars are the standard deviations of the measurement results.

(E) Thermal conductivities of different porous materials and corresponding VIA.

(F) Thermal conductivity of VIA after repeated bending, followed by puncture damage.

(G) Comparison of VIA with existing insulation materials, in terms of the standard thermal-insulation performance metric (R value per inch).

(H and I) Infrared imaging of the top-surface temperature of the insulation material above a low-temperature metal plate for foam insulation (H) and a VIA that is cut along one column of cells (I). Both insulation materials have a thickness of 3.3 mm.

(J and K) Infrared imaging of the top-surface temperature of a trapezoidal insulation material on a cold metal plate for foam insulation (J) and for a reassembled VIA (K), with a material thickness about 6.5 mm. The cutting and reassembly from the square to the trapezoid shape is indicated in the inset in (K). Two VIAs are stacked together with their assembly lines (indicated by arrows) mismatched.

1 year shows that cells adjacent to the damaged region indeed have higher thermal conductivities (Figure S6D), suggesting that the degradation in insulation performance due to vacuum loss is limited to a local area.

Our VIA design is applicable to different core materials, including aerogel composites, pressed powder board (fumed silica), fibrous materials (fiberglass, mineral wool, and cellulose), and foams (Figure 3E). For all these materials, VIA greatly reduces their thermal conductivity to 0.006–0.01 W/m-K and is able to maintain the ultralow thermal conductivity after damage. The different thermal conductivities are mainly due to the different characteristic pore sizes (Figure S7), as a higher vacuum level is required to suppress the gaseous heat conduction for materials with larger pore size (Figure S8) based on the Knudsen's law.[29] This is because, for larger

characteristic pore sizes, a higher vacuum level is needed to increase the mean free path of air molecules above the pore size. When the air mean free path is larger than the pore size, the air molecules experience frequent collisions with the porous structure and the air's contribution to total thermal conductivity largely decreases. For example, because aerogel composite has smaller characteristic pore size than fiberglass, a pressure of 1.0 mbar is needed for the aerogel composite samples, while a pressure of 0.1 mbar would be ideal for fiberglass core material. General vacuum level requirements for other core materials can be found in literature about vacuum insulation panels on the selection of core materials.[30] We also note that core materials in general do not need to be structurally strong to be used in VIA. The core materials will collapse in size somewhat under vacuum. However, the porous structures are not fully packed microscopically, creating gaps in between that are sufficient for vacuum insulation purposes.

The VIA also has a certain flexibility and can be bent without losing its insulation performance. Figure 3F shows that the thermal conductivity of a square VIA remains low after 100 bendings and is not affected by a puncture damage afterward. Here we caution that this test does not justify VIA as a flexible material. While VIA exhibits certain bending flexibility (see supplemental information; Figure S9), severe bending can lead to breakage between the components. This in general would not be a major concern for applications because flat panels are the most common types for thermal insulation. The built environment may involve other types of loading, especially in extreme weather conditions such as strong winds. Nonetheless, thermal-insulation materials are not used as load-bearing structures and generally suffer less from the variations in loads. While the variations in loads may cause excess pressing on VIA materials, pressing is generally less of a concern than bending, because the long-term performance of VIA depends on the hermetic sealing of the structure, which is most affected by shear forces that may lead to breakage between the components. The above damage-resilience and mechanical-bending test illustrate that our VIA provides similar installation convenience and adaptability as conventional insulation materials, while achieving insulation performance 4 times better than that of conventional insulation materials (Figure 3G). While the best aerogels have thermal conductivities of 0.009 W/m-K,[26] this requires careful optimization of the synthesis procedure, and most studies reported thermal conductivities in the range of 0.012—0.02 W/m-K for aerogels.[20,21] Considering this, VIA provides an insulation performance which is twice that of aerogels on average while being more mechanically robust.

To demonstrate the installation convenience of VIA as thermal superinsulation materials for practical applications, we conducted thermal-insulation tests for both damaged and reassembled VIA. In the first test, we study how damaged VIAs protect from an extremely cold object (a metal plate cooled to about −100°C by liquid nitrogen). When conventional foam insulation is placed on the metal plate, the top surface rapidly decreases to below 0°C within 1 min (Figures 3H and S10A). In comparison, the temperature of a damaged VIA material (e.g., one column of arrays is cut off) stays around 20°C for 1 min in undamaged areas (Figures 3I and S10B). The infrared images also clearly demonstrate the vacuum protection by the VIA structure—the undamaged areas have uniformly higher temperatures than those damaged areas. Next, we illustrate how a square VIA can be reshaped into a trapezoid and compare its insulation performance with foam insulations. Both materials are placed on a metal plate cooled to 10°C by a thermoelectric cooler. Assuming that the heat transfer coefficient with the environment is similar, materials with better thermal insulation will exhibit higher top-surface temperatures. Here we stacked two

layers of VIA with one VIA flipped horizontally to minimize the edge heat conduction. Infrared imaging shows that reassembled VIA achieves higher temperatures than the foam insulation (Figures 3J and 3K), much closer to the environmental temperature (Figure S11A). We also used the guarded hot plate setup to measure the average thermal conductivity over a larger area, indicated by the dashed line in Figures 3J and 3K. The thermal conductivity of foam insulation is consistent with the heat flow-meter measurement, while the assembled VIA has a smaller thermal conductivity (Figure S11B). Because the selected area includes the envelope edges and damaged cells, this result represents a worst-case scenario. For a practical VIA with a larger size, we expect most areas will have much lower thermal conductivities.

Application in transportation and building sectors

Lastly, we studied the energy-saving potential of VIA as thermal superinsulation material using transportation and building sectors as examples. In the cold-chain industry, a significant challenge is maintaining a low temperature during transportation, especially when the temperature needed is extremely low. An example is vaccines that need to be maintained below −60°C. In such cases, thermal insulation becomes particularly important[37] (Figure 4A). Compared with foam materials that are currently used for passive insulation, VIA provides significantly better insulation performance. We built a storage box wrapped by insulation materials of the same thickness (Figure 4B). To further reduce the radiative heat transfer with the environment, reference insulation materials (foams) are covered with aluminum foils. Phase-change materials (ice or dry ice) are added to mimic thermal mass. Compared with conventional foam insulation materials, VIA can increase the storage time by about three times for storage near 0°C (Figure 4C). This improvement is not affected even when two sides (front and back) of the storage box are punctured. For storage at much lower temperatures, the increase is less pronounced because the foam material itself has a lower thermal conductivity due to longer air mean free path at lower temperatures. Nonetheless, if we set −80°C to −60°C to be the safe temperature range for storage, VIA still increases the storage time by about 60%, a significant improvement over conventional material (Figure 4D). We have also compared VIA with an aerogel composite-based insulation material (i.e., the core material we use in VIA but without vacuum) covered with aluminum foil. The results show that VIA can increase the storage time by about 50% for storage near 0°C and by about 20% at −80°C to −60°C range (Figure S12), demonstrating VIA's energy-saving advantage in cold transportation.

Significant energy savings are also achievable in the building sector if VIA is added to existing building envelopes to increase thermal insulation (Figures 4E and 4F). We studied annual heating- and cooling-energy consumption for a single-family house in the United States[38] (experimental procedures). Figure 4G shows the temperature of the attic when only the living area is maintained at the setpoint. For the standard house model, the attic temperature is significantly lower than the setpoint. After introducing the thermal insulation—2-cm-thick VIA, with a thermal conductivity of 0.007 W/m-K, is added into the wall and roof—the average attic temperature is increased to around 15°C, and temperature fluctuations are also largely reduced. We further analyzed the annual heating- and cooling-energy savings due to the additional VIA. Heating needs typically account for a significant share of the total household energy use, from below 10% in hotter climates to over 40% in colder areas (Figure 4H). If 2-cm-thick VIA is added to the wall and roof, the annual heating-energy use can be reduced by about 30%–70% (Figure 4H). Similarly, the annual cooling-energy use is reduced by about 10%–25% (Figure 4I). Together, they achieve 20%–40% reduction in total energy use for space heating and cooling, and annual energy savings of 4–13 GJ per household. A thicker thermal-insulation layer can lead to even

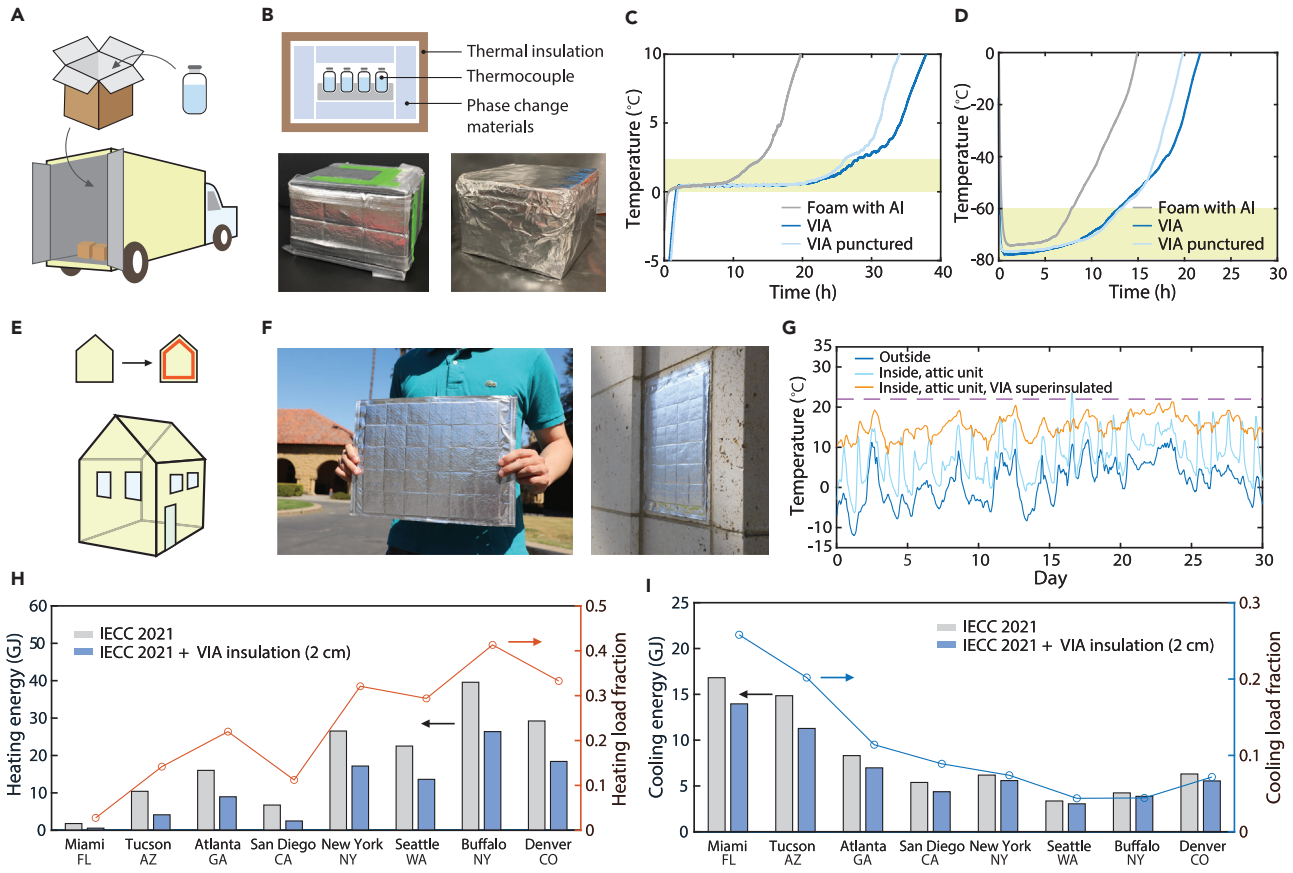

Figure 4. Application in cold transportation and building thermal envelope

(A) Passive ultrahigh thermal insulation can significantly increase the storage time for objects (e.g., vaccines) requiring storage at low temperatures, saving cooling energy.

(B) A home-built cold-storage box, with the outside wrapped with insulation materials and the inside filled with phase-change materials. Ice and dry ice are tested for different storage temperature ranges.

(C and D) Inside-box temperature variation with different insulation materials, with ice (C) and dry ice (D) being the phase-change materials. The shaded area indicates the desired temperature range for storage.

(E) Ultrahigh thermal insulation can significantly increase buildings' thermal insulation and improve their energy efficiency.

(F) Pictures of a large vacuum insulation array and its attachment on building walls.

(G) Simulated temperature variation of an attic unit in a single-family house at New York during winter. For the insulated case, a 2-cm-thick wall with a thermal conductivity of 0.007 W/m-K is added to each heat transfer surface of the house.

(H and I) Energy-saving analysis of annual heating-energy (H) and cooling-energy consumption (I) in a single-family house across the United States.

greater energy savings. For example, 5–18 GJ can be saved if 5-cm-thick VIA is added to the house (Figure S13). Increasing the insulation thickness also implies higher initial investment, and we have provided a cost analysis for VIA based on literature information about the cost of vacuum insulation panels[39] (see supplemental information). The above analysis suggests that adding a thin thermal superinsulation layer to the existing building envelope is an effective way to mitigate CO_2 emissions, with a potential annual emission reduction on the order of 1 Gt.

DISCUSSION

In summary, we designed and fabricated a thermal superinsulation structure that combines the installation convenience of conventional insulation materials and the ultrahigh thermal-insulation performance of vacuum insulation panels. The key concept of this design is a hermetically sealed vacuum insulation array, or VIA, which creates local vacuum insulations that are separated from each other by gas-barrier

films. This design allows our insulation material to be punctured, cut, bent, and reassembled without losing its insulation performance. This design concept is applicable to various porous insulation core materials and is compatible with existing manufacturing processes, such as roll-to-roll manufacturing of polymeric laminate films. VIAs can help achieve energy savings in different areas from cold transportation to building-space heating and cooling, but we also note that different applications have different requirements for the duration over which a high insulation performance is maintained. While we have experimentally demonstrated the long-term thermal-insulation performance of VIA, applications in the built environment require high insulation performance over a much longer duration (e.g., 20 years) and represent one of the most challenging areas for thermal insulation. In this respect, more characterizations regarding the long-term aging behavior would be needed to project VIA's high insulation performance over longer terms. For example, moisture in the building environment can also affect the thermal performance of insulation materials. While EVOH itself does not have sufficiently high moisture-barrier performance, laminates of EVOH and other polymers such as PE can help to achieve better overall barrier performance even under humid conditions due to the combined advantages of EVOH's low oxygen permeation rates and PE's low moisture permeation rates.[34,36] Besides, flammability is also an important factor to consider for building applications. While typical core materials such as fumed silica and fiberglass are not flammable, the flammability of VIA also depends on the gas-barrier materials, which are polymeric films and categorized as flammable. Nonetheless, the gas-barrier component is a small fraction of the VIA and the flammability can be improved by addition of fire retardants. We believe that additional optimization mentioned above will allow VIAs to meet international standard requirements for thermal-insulation materials, such as ISO/DIS 16478, which is specified for vacuum insulation panels, for VIAs to be adopted in practical applications, helping to improve the energy efficiency as well as reduce the energy consumptions and CO_2 emissions.

EXPERIMENTAL PROCEDURES

Resource availability

Lead contact

Further information and requests for resources and materials should be directed to the lead contact, Yi Cui (yicui@stanford.edu).

Material availability

The materials in this study will be made available upon reasonable request.

Data and code availability

All data are present in the paper and supplemental information.

Material and fabrication

The porous core material used as demonstration for our VIA is an aerogel-based composite (Spaceloft blanket, Aspen Aerogels). The envelope film (Protect 470, Protective Packaging Corporation) is an aluminum-based laminate film, with a thin PE sealing layer on one side, and an oriented polypropylene layer on the other side for protection. The nylon barrier film (chamber pouches, VacMaster) has a thin PE layer on one side. The EVOH barrier film (Polynova) has PE sealing layers on both sides. Other core materials, such as fumed silica, fiberglass mat, mineral wool, and loose cellulose are commercially available conventional insulation materials and are obtained from online market. The foam is a polymeric melamine foam traditionally used for cleaning purposes.

The vacuum insulation array structure is made following the vacuum sealing-heat pressing process. First, the core materials are cut into identical sizes and assembled with gas-barrier structure and two envelopes (top and bottom) together. Each core material is covered with the gas-barrier material by folding the gas-barrier material around the core. For most discussions in this study, each cell has a size of 3.8 × 3.8 cm^2. A larger cell size can give a lower overall thermal conductivity, but this is limited by the heating plate size of our heat-pressing equipment. Second, the two envelopes are sealed together under vacuum. For vacuum sealing, we use a household vacuum sealer (VacMaster) but modified it by separating its vacuum pumping and heat-sealing steps. The pressure level provided by the internal vacuum pump of the sealer is not sufficiently low. Instead, we have re-routed the pumping path to a high-power vacuum pump that allows us to pump the pressure down to less than 0.5 mbar. After the desired low pressure is reached, we will then execute the program to heat seal the sample. After the structure is taken out from the vacuum, it is then pressed between hot plates at about 130°C for 60 s. The heat-pressing temperature needs to be slightly higher than the melting point of the sealing layer (PE in our case), and we have found 130°C is sufficient for us to achieve satisfying sealing results. The pressing time required to achieve good sealing depends on two aspects. First, heat takes time to penetrate the sample and heat up the regions surrounding the sealing layers. Second, the polymers also need certain time to allow themselves to diffuse. For gas-barrier films with similar thickness and with same materials as the sealing layer, we expect the required duration would be similar. In general, we found that 1 min is sufficient to achieve good sealing for both nylon and EVOH barrier films. The heat-pressing step depends mostly on the gas-barrier material and is not sensitive to the type of core materials. The heat-pressing step ensures the gas-barrier structure and the envelopes are hermetically sealed together.

Thermal-conductivity measurement

The thermal conductivity of different insulation materials is measured using the heat flowmeter method. The insulation material is placed in between two aluminum plates, whose temperatures are controlled by thermoelectric plates and set to 13°C and 33°C (with an average temperature close to the room temperature). Two thermocouples are embedded in the aluminum plates, near the surfaces close to the insulation materials. A heat flux sensor (FHF03, Hukseflux) with an effective sensing area of 2.5 cm^2 is mounted within the bottom aluminum plate. A proportional-integral-derivative (PID) control algorithm is used to stabilize the temperatures of the aluminum plates at the setpoint (within 0.05°C) and the data are obtained only after the temperatures are stabilized. The thermal conductivity is calculated based on $k = (VSt)/\Delta T$, where V is the voltage output of the heat flux sensor, S is its sensitivity (W/m^2V), t is the insulation material thickness, and ΔT is the temperature difference between two aluminum plates. The setup has been calibrated against reference materials and the obtained thermal conductivities are in good agreement with literature for different materials, including air. The picture of the setup and calibration details can be found in Figure S2.

We note that there are two common techniques for characterizing thermal-insulation materials—guarded hot plate method and heat flowmeter method. Unlike guarded hot plate method, the heat flowmeter method is less sensitive to parasitic heat transfer as long as the sample size is much larger than the heat flux sensor and the lateral dimension of the sample is much larger than its thickness. Our measured thermal conductivity includes contact thermal resistance, and therefore is a conservative estimation of the sample's actual thermal conductivity. The contact thermal resistance mainly comes from the air gap, which has a thermal conductivity much larger than the sample

of interest in this study. Moreover, the contribution of contact thermal resistance can be further reduced by slightly pressing the upper aluminum plate to minimize the air gap. Therefore, the contact thermal resistance only introduces a negligible error in the thermal-conductivity measurement (an estimation about the error introduced by the contact thermal resistance is given in supplemental information).

Due to the limited sensing area of the heat flux sensor, the heat flowmeter method above essentially measures the average thermal conductivity around the sensing area. In order to characterize the average thermal conductivity across a larger area (for reassembled VIA), we have also built a guarded hot plate setup (schematic shown in Figure S4). The hot plate has an area of $A = 10 \times 10\ \mathrm{cm}^2$, and is heated by an attached thin film heater. The heating power Q mainly goes through the insulation material, and the average thermal conductivity is obtained by $k = (Qt)/(A\Delta T)$.

Thermal modeling

In order to determine the material requirement for the gas-barrier structure, we performed thermal modeling to study the total thermal conductivity of VIA structure with different unit cell dimensions and gas-barrier material properties. An infinite square vacuum cell array is studied with periodic boundary conditions in x-y direction. The height of the insulation structure is 3.6 mm, and the width of the gas-barrier structure that separates adjacent cells is 200 μm (gas-barrier films have 100 μm thickness, and two films are pressed together between adjacent cells). The thermal conductivity of the core material is taken to be 0.005 W/m-K. Two metal plates are placed on two sides, in direct contact with the insulation materials. The metal plates are maintained at two different temperatures. The average thermal conductivity k is calculated based on $k = (Qt)/(A\Delta T)$, where Q is the total heat flow through one unit cell, t is the thickness of the insulation material, A is the area of one unit cell, and ΔT is the temperature difference between two metal plates.

Long-term gas permeation analysis

Gas permeation in general can happen via two routes—one is directly through the gas-barrier material, and the other through the sealings. Past aging studies on vacuum insulation panels have suggested that the permeation through sealings is often dominant and the permeation rate per unit length is around $0.002 - 0.009\mathrm{cm}^3/(\mathrm{m}\cdot\mathrm{day}\cdot\mathrm{atm})$.[40] If we take an average value ($0.005\mathrm{cm}^3/(\mathrm{m}\cdot\mathrm{day}\cdot\mathrm{atm})$) and regard it as the permeation rate for air, the total permeation rate into one cell for unit pressure difference is then $R \approx 0.0003\mathrm{cm}^3/(\mathrm{day}\cdot\mathrm{atm})$, assuming a unit cell dimension of $5 \times 5 \times 0.1\ \mathrm{cm}^3$. When one cell loses vacuum, only the neighboring cells are immediately affected (see schematic in Figure S5B). The local pressure p_1 in the neighboring cells labeled as 1 follows $\frac{dp_1}{dt} = \frac{R}{V}(p_0 - p_1)$, where V is the cell volume, and p_0 is the atmospheric pressure. For cells labeled as 2 which are slightly further away (Figure S5B), the pressure p_2 follows approximately $\frac{dp_2}{dt} = \frac{R}{V}(p_1 - p_2)$. Figure S6C shows the expected pressure rise as a function of time up to 20 years in cells at different locations from the punctured site. The results show that at more than two cells away from the punctured site, the pressure rise for a 10-year span is less than 10 mbar, which is sufficient to maintain the core material to have a low thermal conductivity in the long term.

Passive cold-storage test

For the cold-storage test, a small paper box is wrapped around by insulation materials of the same thickness. Two phase-change materials are used (ice and dry ice) to study storage at different temperature ranges. The same weight of phase-change materials (750 g) is added to foam insulated box and VIA insulated box, to mimic

a given amount of thermal mass. A vial filled with water is placed inside the box and the temperature of the vial is monitored by an attached thermocouple to study the temperature variation of stored item during cold storage.

Building energy saving analysis

The annual heating-energy consumption in a single-family house at different locations within the United States is modeled using EnergyPlus. The single-family house model is taken from the literature and contains two separate units (one living unit and one attic unit).[38] This standard house model is built mainly based on 2021 International Energy Conservation Code. The air leakage rates are changed to zero to reflect an air-tight condition. Weather data for different cities are given as input, and heating/cooling power is constantly adjusted to maintain the temperature of the living unit at the setpoint. The VIA insulated condition further adds a 2 cm thick thermal-insulation layer of 0.007 W/m-K thermal conductivity to each heat transfer surface of the house (wall and roof). Annual heating-energy consumption is obtained by summing up all heating-energy uses throughout the year.

SUPPLEMENTAL INFORMATION

Supplemental information can be found online at https://doi.org/10.1016/j.joule.2022.07.015.

ACKNOWLEDGMENTS

The authors thank Y. Ye and R. Xu for the discussions on the manufacturing process. Part of this work was performed at the Stanford Nano Shared Facilities (SNSF), supported by the National Science Foundation under award ECCS-1542152. Y.C. acknowledges the support from the Future Investment Initiative Institute.

AUTHOR CONTRIBUTIONS

J.Z. and Y.C. conceived the project. J.Z. and J.X. built the thermal-conductivity measurement setup. J.Z. conducted the thermal modeling, fabricated the vacuum insulation structure, and tested its thermal and mechanical properties, with help from Y.P., Y.W., Z.H., and X.X. J.Z. and Y.P. analyzed the building energy savings based on the measured material properties. All authors commented on, discussed, and edited the manuscript.

DECLARATION OF INTERESTS

The authors declare no competing interests.

Received: March 11, 2022
Revised: June 13, 2022
Accepted: July 29, 2022
Published: August 23, 2022

REFERENCES

1. Yang, L., Yan, H., and Lam, J.C. (2014). Thermal comfort and building energy consumption implications – a review. Appl. Energy *115*, 164–173. https://doi.org/10.1016/j.apenergy.2013.10.062.

2. IEA (2019). Global Status Report for Buildings and Construction 2019. https://www.iea.org/reports/global-status-report-for-buildings-and-construction-2019.

3. Laustsen, J. (2008). Energy efficiency requirements in building codes, energy efficiency policies for new buildings. IEA Information Paper. https://www.iea.org/reports/energy-efficiency-requirements-in-building-codes-policies-for-new-buildings.

4. Wright, G.S., and Klingenberg, K. (2015). Climate-Specific Passive Building Standards (National Renewable Energy Laboratory). https://doi.org/10.2172/1220516.

5. Strand, M.T., Hernandez, T.S., Danner, M.G., Yeang, A.L., Jarvey, N., Barile, C.J., and McGehee, M.D. (2021). Polymer inhibitors enable >900 cm^2 dynamic windows based on reversible metal electrodeposition with high solar modulation. Nat. Energy *6*, 546–554. https://doi.org/10.1038/s41560-021-00816-7.

6. Davy, N.C., Sezen-Edmonds, M., Gao, J., Lin, X., Liu, A., Yao, N., Kahn, A., and Loo, Y.-L. (2017). Pairing of near-ultraviolet solar cells with electrochromic windows for smart management of the solar spectrum. Nat.

Energy *2*, 1–11. https://doi.org/10.1038/nenergy.2017.104.

7. Wang, S., Jiang, T., Meng, Y., Yang, R., Tan, G., and Long, Y. (2021). Scalable thermochromic smart windows with passive radiative cooling regulation. Science *374*, 1501–1504. https://doi.org/10.1126/science.abg0291.

8. Lin, J., Lai, M., Dou, L., Kley, C.S., Chen, H., Peng, F., Sun, J., Lu, D., Hawks, S.A., Xie, C., et al. (2018). Thermochromic halide perovskite solar cells. Nat. Mater. *17*, 261–267. https://doi.org/10.1038/s41563-017-0006-0.

9. Wheeler, L.M., Moore, D.T., Ihly, R., Stanton, N.J., Miller, E.M., Tenent, R.C., Blackburn, J.L., and Neale, N.R. (2017). Switchable photovoltaic windows enabled by reversible photothermal complex dissociation from methylammonium lead iodide. Nat. Commun. *8*, 1722. https://doi.org/10.1038/s41467-017-01842-4.

10. Strobach, E., Bhatia, B., Zhao, L., and Wang, E.N. (2018). Thermal performance of high-efficiency window technologies. Annu. Rev. Heat Transf. *21*, 59–97. https://doi.org/10.1615/AnnualRevHeatTransfer.2019030886.

11. Zhong, Y., Kou, R., Chen, R., and Qiao, Y. (2021). Window+: electrostatic levitation enabled polymer-air multilayer (EPAM) structures for highly transparent energy efficient windows. Energy Convers. Manag. *248*, 114803. https://doi.org/10.1016/j.enconman.2021.114803.

12. Raman, A.P., Anoma, M.A., Zhu, L., Rephaeli, E., and Fan, S. (2014). Passive radiative cooling below ambient air temperature under direct sunlight. Nature *515*, 540–544. https://doi.org/10.1038/nature13883.

13. Zhai, Y., Ma, Y., David, S.N., Zhao, D., Lou, R., Tan, G., Yang, R., and Yin, X. (2017). Scalable-manufactured randomized glass-polymer hybrid metamaterial for daytime radiative cooling. Science *355*, 1062–1066. https://doi.org/10.1126/science.aai7899.

14. Mandal, J., Fu, Y., Overvig, A.C., Jia, M., Sun, K., Shi, N.N., Zhou, H., Xiao, X., Yu, N., and Yang, Y. (2018). Hierarchically porous polymer coatings for highly efficient passive daytime radiative cooling. Science *362*, 315–319. https://doi.org/10.1126/science.aat9513.

15. Li, T., Zhai, Y., He, S., Gan, W., Wei, Z., Heidarinejad, M., Dalgo, D., Mi, R., Zhao, X., Song, J., et al. (2019). A radiative cooling structural material. Science *364*, 760–763. https://doi.org/10.1126/science.aau9101.

16. Tang, K., Dong, K., Li, J., Gordon, M.P., Reichertz, F.G., Kim, H., Rho, Y., Wang, Q., Lin, C.-Y., Grigoropoulos, C.P., et al. (2021). Temperature-adaptive radiative coating for all-season household thermal regulation. Science *374*, 1504–1509. https://doi.org/10.1126/science.abf7136.

17. U.S. Dept. of Energy, and Office of Energy Efficiency and Renewable Energy. (2020). Research and development opportunities report for opaque building envelopes. https://www.energy.gov/eere/buildings/downloads/research-and-development-opportunities-report-opaque-building-envelopes.

18. Schiavoni, S., D'Alessandro, F., Bianchi, F., and Asdrubali, F. (2016). Insulation materials for the building sector: a review and comparative analysis. Renew. Sustain. Energy Rev. *62*, 988–1011. https://doi.org/10.1016/j.rser.2016.05.045.

19. Fraleoni-Morgera, A., and Chhikara, M. (2019). Polymer-based nano-composites for thermal insulation. Adv. Eng. Mater. *21*, 1801162. https://doi.org/10.1002/adem.201801162.

20. Baetens, R., Jelle, B.P., and Gustavsen, A. (2011). Aerogel insulation for building applications: a state-of-the-art review. Energy Build *43*, 761–769. https://doi.org/10.1016/j.enbuild.2010.12.012.

21. Cuce, E., Cuce, P.M., Wood, C.J., and Riffat, S.B. (2014). Toward aerogel based thermal superinsulation in buildings: a comprehensive review. Renew. Sustain. Energy Rev. *34*, 273–299. https://doi.org/10.1016/j.rser.2014.03.017.

22. Shimizu, T., Kanamori, K., and Nakanishi, K. (2017). Silicone-based organic–inorganic hybrid aerogels and xerogels. Chemistry *23*, 5176–5187. https://doi.org/10.1002/chem.201603680.

23. Lu, X., Arduini-Schuster, M.C., Kuhn, J., Nilsson, O., Fricke, J., and Pekala, R.W. (1992). Thermal conductivity of monolithic organic aerogels. Science *255*, 971–972. https://doi.org/10.1126/science.255.5047.971.

24. Wicklein, B., Kocjan, A., Salazar-Alvarez, G., Carosio, F., Camino, G., Antonietti, M., and Bergström, L. (2015). Thermally insulating and fire-retardant lightweight anisotropic foams based on nanocellulose and graphene oxide. Nat. Nanotechnol. *10*, 277–283. https://doi.org/10.1038/nnano.2014.248.

25. Li, T., Song, J., Zhao, X., Yang, Z., Pastel, G., Xu, S., Jia, C., Dai, J., Chen, C., Gong, A., et al. (2018). Anisotropic, lightweight, strong, and super thermally insulating nanowood with naturally aligned nanocellulose. Sci. Adv. *4*, eaar3724. https://doi.org/10.1126/sciadv.aar3724.

26. Cohen, E., and Glicksman, L. (2015). Thermal properties of silica aerogel formula. J. Heat Transf. *137*, 081601. https://doi.org/10.1115/1.4028901.

27. Xu, X., Zhang, Q., Hao, M., Hu, Y., Lin, Z., Peng, L., Wang, T., Ren, X., Wang, C., Zhao, Z., et al. (2019). Double-negative-index ceramic aerogels for thermal superinsulation. Science *363*, 723–727. https://doi.org/10.1126/science.aav7304.

28. Bouquerel, M., Duforestel, T., Baillis, D., and Rusaouen, G. (2012). Heat transfer modeling in vacuum insulation panels containing nanoporous silicas—a review. Energy Build *54*, 320–336. https://doi.org/10.1016/j.enbuild.2012.07.034.

29. Knudsen, M. (1911). Die molekulare Wärmeleitung der Gase und der Akkommodationskoeffizient. Ann. Phys. *339*, 593–656. https://doi.org/10.1002/andp.19113390402.

30. Baetens, R., Jelle, B.P., Thue, J.V., Tenpierik, M.J., Grynning, S., Uvsløkk, S., and Gustavsen, A. (2010). Vacuum insulation panels for building applications: a review and beyond. Energy Build *42*, 147–172. https://doi.org/10.1016/j.enbuild.2009.09.005.

31. Kosny, J., and Yarbrough, D. (2018). Recent advances in vacuum thermal insulations used in building thermal envelopes. Annu. Rev. Heat Transf. *21*, 25–57. https://doi.org/10.1615/AnnualRevHeatTransfer.2019030270.

32. Simmler, H., Brunner, S., Heinemann, U., Schwab, H., Kumaran, K., Mukhopadhyaya, P., Quenard, D., Sallee, H., Noller, K., Kuecuekpinar-Niarchos, E., et al. (2005). Vacuum insulation panels – study on VIP-components and panels for service life prediction of VIP in building applications (Subtask A). https://www.osti.gov/etdeweb/biblio/21131463.

33. Gonçalves, M., Simões, N., Serra, C., and Flores-Colen, I. (2020). A review of the challenges posed by the use of vacuum panels in external insulation finishing systems. Appl. Energy *257*, 114028. https://doi.org/10.1016/j.apenergy.2019.114028.

34. Lange, J., and Wyser, Y. (2003). Recent innovations in barrier technologies for plastic packaging—a review. Packag. Technol. Sci. *16*, 149–158. https://doi.org/10.1002/pts.621.

35. Zhang, Z., Britt, I.J., and Tung, M.A. (2001). Permeation of oxygen and water vapor through EVOH films as influenced by relative humidity. J. Appl. Polym. Sci. *82*, 1866–1872. https://doi.org/10.1002/app.2030.

36. Maes, C., Luyten, W., Herremans, G., Peeters, R., Carleer, R., and Buntinx, M. (2018). Recent updates on the barrier properties of ethylene vinyl alcohol copolymer (EVOH): a review. Polym. Rev. *58*, 209–246. https://doi.org/10.1080/15583724.2017.1394323.

37. Chen, S.-I., Norman, B.A., Rajgopal, J., and Lee, B.Y. (2015). Passive cold devices for vaccine supply chains. Ann. Oper. Res. *230*, 87–104. https://doi.org/10.1007/s10479-013-1502-5.

38. Mendon, V.V., Selvacanabady, A., Zhao, M., and Taylor, Z.T. (2015). National Cost-Effectiveness of the Residential Provisions of the 2015 IECC (Pacific Press Northwest National Laboratory). https://doi.org/10.2172/1773019.

39. Fantucci, S., Garbaccio, S., Lorenzati, A., and Perino, M. (2019). Thermo-economic analysis of building energy retrofits using VIP - vacuum insulation panels. Energy Build *196*, 269–279. https://doi.org/10.1016/j.enbuild.2019.05.019.

40. Wegger, E., Jelle, B.P., Sveipe, E., Grynning, S., Gustavsen, A., Baetens, R., and Thue, J.V. (2011). Aging effects on thermal properties and service life of vacuum insulation panels. J. Build. Phys. *35*, 128–167. https://doi.org/10.1177/1744259111398635.

Joule, Volume *6*

Supplemental information

Vacuum insulation arrays as damage-resilient thermal superinsulation materials for energy saving

Jiawei Zhou, Yucan Peng, Jinwei Xu, Yecun Wu, Zhuojun Huang, Xin Xiao, and Yi Cui

Supplemental Experimental Procedures

Gas barrier performance quantification of polymer films

Based on the data from the vendors, nylon barrier film has an oxygen permeation rate of about α =45 cm^3/m^2-day, and EVOH barrier film has an oxygen permeation rate of about α =3 cm^3/m^2-day. Usually, nitrogen permeation rate is close to oxygen permeation rate and we will use these as the average permeation rates for air. For a rectangle-shaped sample with one side covered with the gas barrier material (assuming the area is A and thickness is d, and the aluminum envelope has negligible gas leaking rate), the pressure inside after a 30-day time span ($t = 30\ days$) can be estimated as

$$p = \frac{\alpha A t}{A d} = \frac{\alpha t}{d}\ [atm]$$

Given the sample thickness is about 3mm, the estimated pressure is about 0.45 atm (or 450 mbar) for nylon barrier, and about 0.03 atm (or 30 mbar) for EVOH barrier. Based on the thermal conductivity-pressure dependence of the aerogel composite core material (Supplementary Figure 8), this would lead to a thermal conductivity of about 0.01 W/m-K for nylon barrier, and 0.007 W/m-K for EVOH barrier after a 30-day time span. These estimations are consistent with the measured thermal conductivities shown in Fig. 2c. We note that the difference can result from imperfect sealing between gas barrier films and aluminum envelopes and/or the uncertainty in the thermal conductivity-pressure data.

Estimation of thermal conductivity error due to contact resistance

Our measurement set up cannot eliminate the contact thermal resistance. However, for samples with ultralow thermal conductivities, as those of interest in this study, the contact thermal resistance represents a small contribution and can be reduced by slightly pressing the upper aluminum plate downwards to minimize the air gap between the sample and the aluminum plate. An estimation about this is given below.

Assume the sample has a thickness of 3mm and a thermal conductivity of 0.01 W/m-K. The major contact thermal resistance comes from the air gap due to sample's uneven surfaces. By slightly pressing the upper aluminum, the air gap distance can be generally limited to be smaller than 0.1 mm. The measured thermal conductivity includes the contact resistances on the two sides, which can be estimated based on the gap distance and air's thermal conductivity:

$$k_{measure} = \frac{3\text{mm} + 2 \times 0.1\text{mm}}{\frac{3\text{mm}}{0.007\ \text{W/mK}} + 2 \times \frac{0.1\text{mm}}{0.026\ \text{W/mK}}} = 0.0104\ \text{W/mK}$$

The error due to contact thermal resistance is less than 5% and thus represents a small contribution. Moreover, due to contact resistance, the measured thermal conductivity is a conservative estimation and the sample's actual thermal conductivity is lower. We think the contact thermal resistance is not a major issue for our study.

Bending curvature analysis for VIA

Here we provide an estimation about VIA's flexibility based on the radius of curvature when VIA experiences bending forces. As illustrated in Supplementary Figure 9, when VIA's are under bending forces, each cell remains relatively rigid due to vacuum inside, and the bending mainly

occurs at the joints between cells. Through experiments, we have found that the angle θ developed between adjacent cells is usually less than 5 degrees (Supplementary Figure 9, also see inset photo of Fig. 3f). One thus expects that smaller cell size allows one to bend more (more joints), and achieves a smaller radius of curvature. Supplementary Figure 9b shows achievable radius of curvature with respect to cell size assuming the angle θ between adjacent cells is limited to 5 degrees. Also plotted is the total thermal conductivity of VIA assuming mesh material has a thermal conductivity of 0.1 W/m-K (other conditions are the same as those in Fig. 2a). In general, for VIA with a total thermal conductivity less than 7 W/m-K, bending radius of curvature of 20-30 cm is achievable.

Cost analysis for VIA

The major cost for VIA, and similarly for vacuum insulation panels, is associated with raw materials and the manufacturing process. Among them, the porous core materials represent the dominant portion of the total cost. Because the gas barrier mesh only takes a small volume, gas barrier materials will not contribute significantly to the total cost. The heat pressing step can be performed by standard heat pressing equipment and thus does not require significant capital investment either. Therefore, we can use the cost of vacuum insulation panels to estimate the cost of VIAs with different thicknesses. Based on literature, vacuum insulation panels with thickness of 2 cm have a cost on the order of 200 $/m^2, and the cost increases to about 250 $/m^2 for when the thickness increases to 3 cm. As the major cost comes from the core materials, a cost estimation for vacuum insulation panels with thickness of 5 cm will be about 350 $/m^2. Based on this, compared to 2 cm thick VIAs (with a cost about 200 $/m^2), additional cost increase of about 150 $/m^2 is needed if 5 cm thick VIAs are used instead. We mention that these are only estimated values and the actual cost will vary depending on the source of materials and manufacturing details.

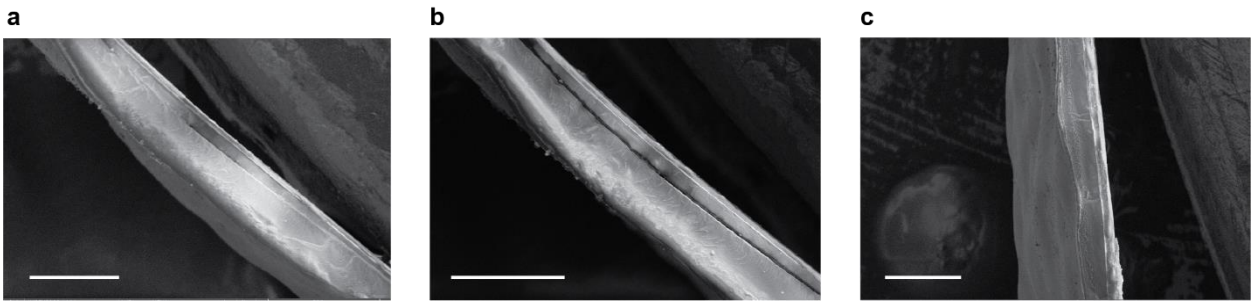

Figure S1. **Cross-sectional SEM images of the sealed regions between nylon barrier film and Al envelope**. (**a-b**) 30 second sealing time. (**c**) 120 second sealing time. The scale bar is 400 μm.

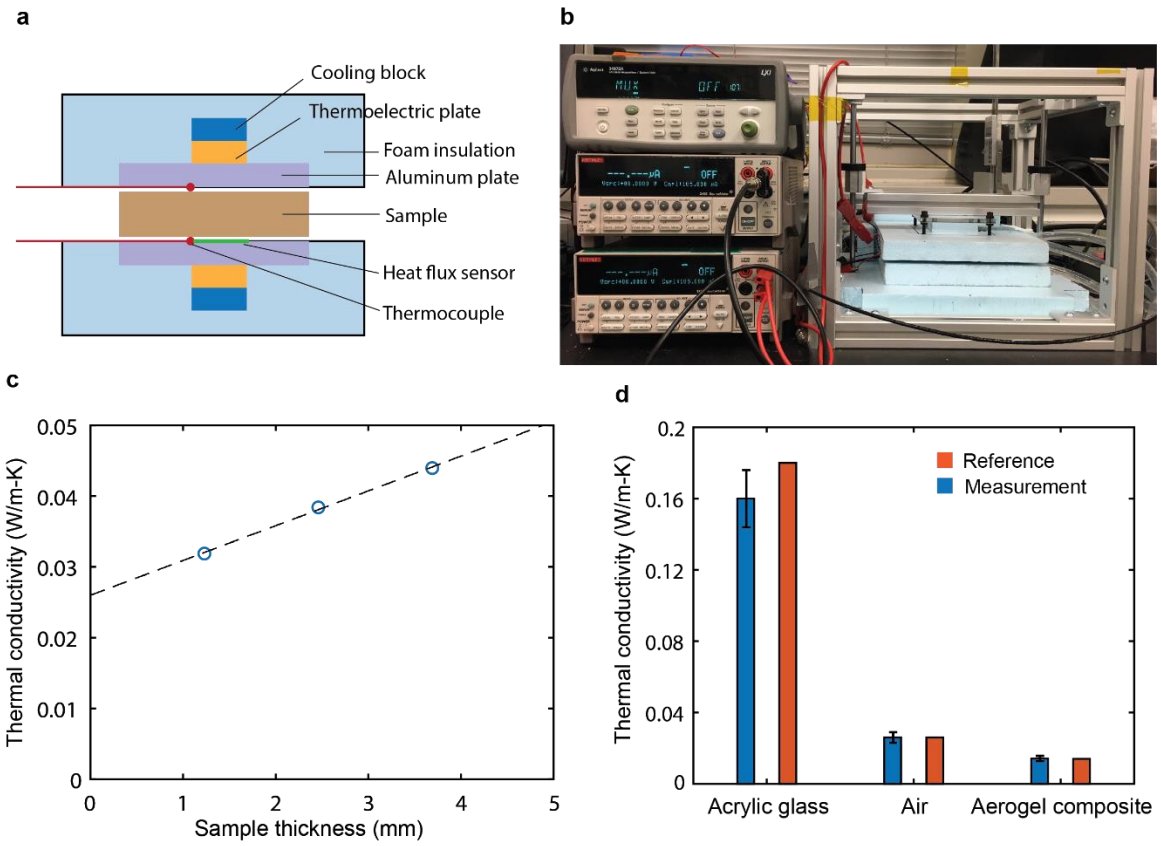

Figure S2. **Thermal conductivity measurement set up**. **a**, Schematic of the set up, based on the heat flowmeter method. The temperatures of the top and bottom aluminum plates are controlled by two thermoelectric plates, whose other sides are cooled by a circulating water bath. The sample thickness is measured by a caliper which records the position of the upper plate. Two thermocouples are embedded to measure the plate temperatures, and a heat flux sensor is embedded in the bottom plate to measure the heat flux. **b**, Photo of the measurement set up. **c**, Apparent thermal conductivity of air at different plate gap distances. The extrapolation to zero gap gives the true thermal conductivity of air, while at finite gap distance thermal radiation also plays a role (from the slope we extracted an average emissivity of about 0.83). **d**, Measured thermal conductivity values for reference samples, including acrylic glass, air, and a commercial aerogel-based composite insulation material.

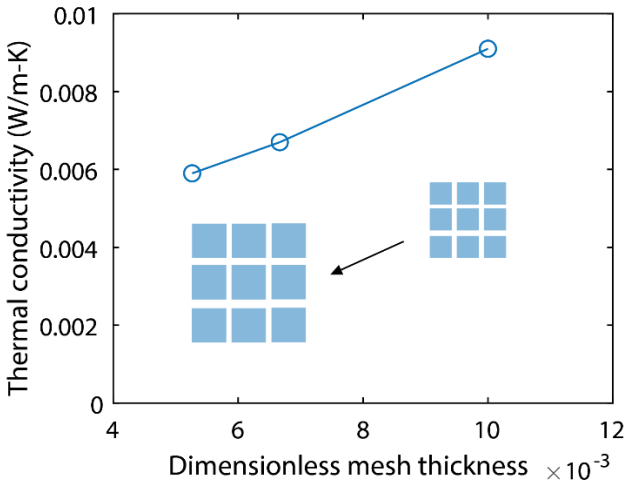

Figure S3. **Thermal conductivity variation of VIA with unit cell size**. The thermal conductivity is measured at the center for a three-by-three square-shape VIA. The dimensionless mesh thickness is defined as the ratio between the thickness of the gas barrier material that separates adjacent unit cells (about 200 μm) and the unit cell length.

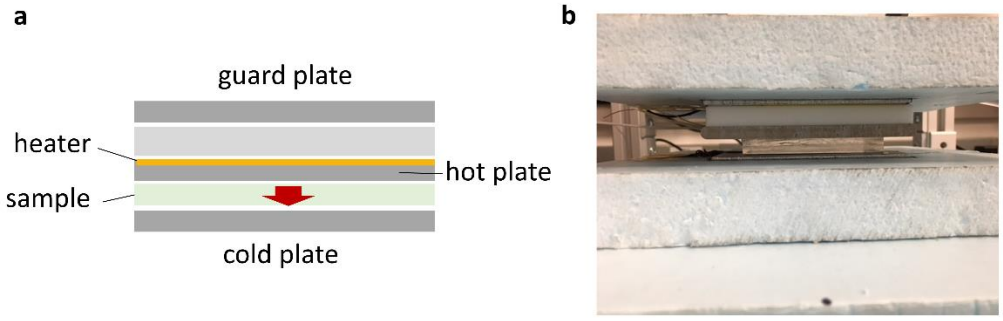

Figure S4. **Guarded hot plate set up**. **a**,The schematic of the guarded hot plate method. The temperature of the hot plate is controlled by an attached thin film heater, and is separated from the guard plate by a foam insulation material. Both guard plate and hot plate are maintained at the same temperature (23 ℃). The plates have an area of $10.2 \times 10.2\ cm^2$. The temperature of the cold plate is set to 13 ℃ and is controlled by a thermoelectric cooler. **b**, Photo of the guarded hot plate set up.

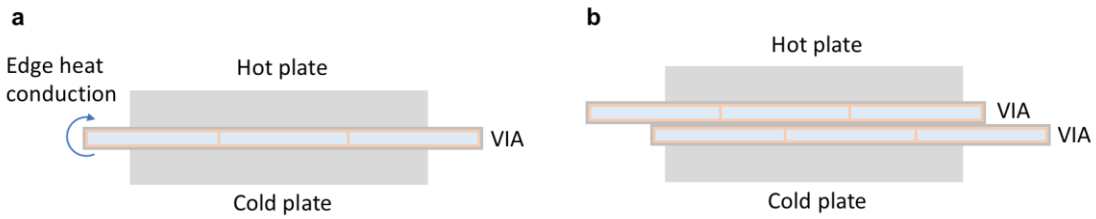

Figure S5. **Thermal conductivity measurement over a larger area. a**, For one VIA layer, owing to the limited size, significant heat conduction occurs at the edge of VIA along the aluminum-based envelope, contributing to the overall thermal conductivity. **b**, When two VIA's are stacked together and their gas barrier mesh structures are mismatched, the edge heat conduction is reduced due to the longer heat conduction contour.

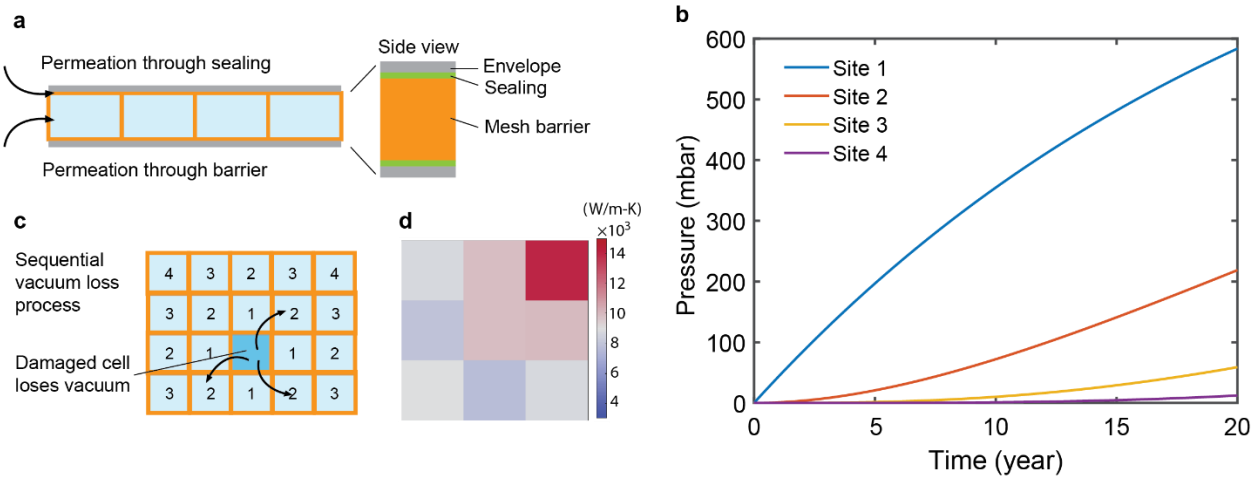

Figure S6. **Long-term gas permeation analysis**. **a**, Schematic of significant vacuum loss channels. **b**, Illustration of the sequential vacuum loss process in the proposed insulation material. **c**, Prediction of pressure rise in the vacuum insulation structure after a perforation damage. **d**, Thermal conductivities at different locations for a three-by-three square VIA with nylon barrier with a corner cell damaged (top-right corner), after one-year span.

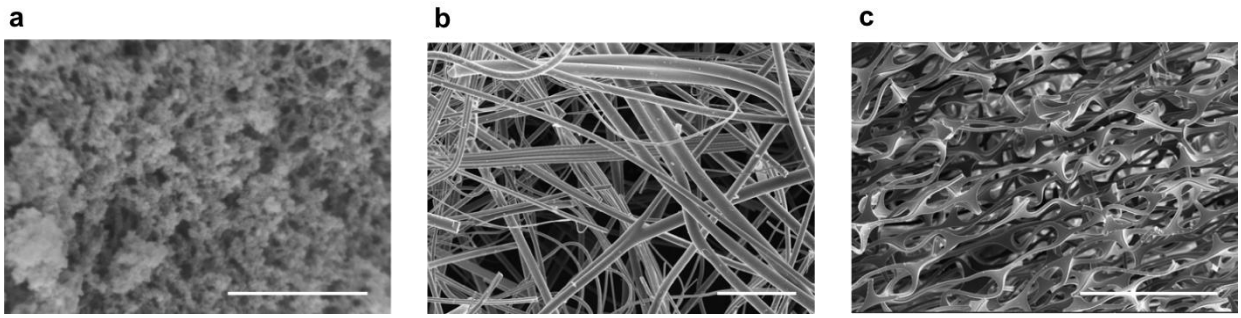

Figure S7. **Scanning electron microscope images of representative core materials**. These materials are used as the core for the vacuum insulation array structure. **a**, Aerogel-based composites. Scale bar is 500 nm. **b**, Fiberglass mat. Scale bar is 50 μm. **c**, Melamine polymeric foam. Scale bar is 200 μm.

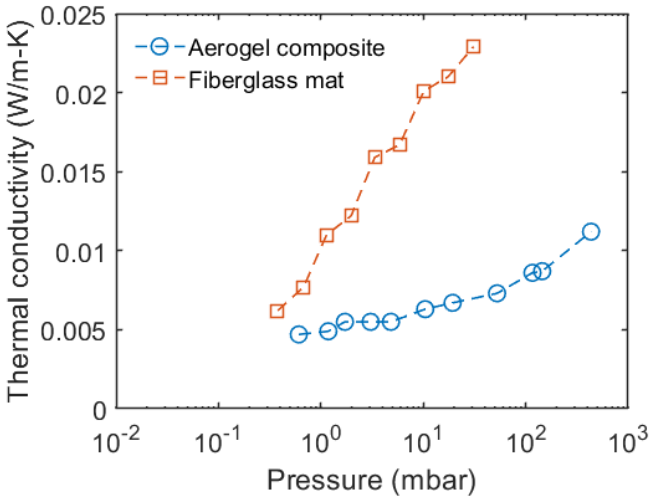

Figure S8. **Thermal conductivity variation with pressure**. The results are measured by sealing the core material at different pressures. Due to the smaller pore size in aerogel based composite core material (typically tens of hundreds of nanometers) compared to fiberglass (a few microns to tens of microns), the thermal conductivity is much less sensitive to the pressure, only showing increases when the pressure increases above 10 mbar.

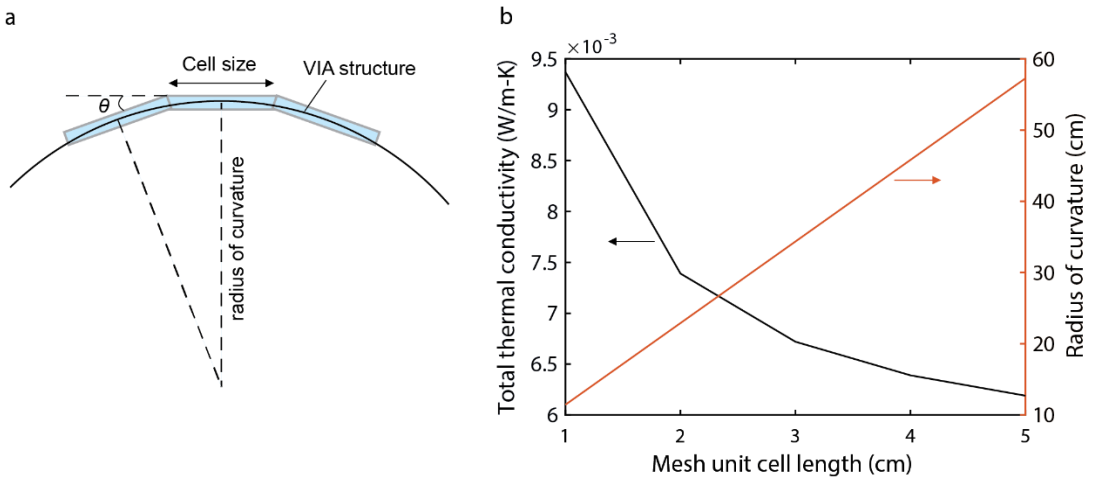

Figure S9. **Analysis about bending curvature of VIA**. **a**, Illustration of VIA under bending forces. **b**, Bending radius of curvature with respect to mesh unit cell length, plotted together with VIA's total thermal conductivity. We assume the angle θ between adjacent cells is limited to 5 degrees and the mesh material has a thermal conductivity of 0.1 W/m-K.

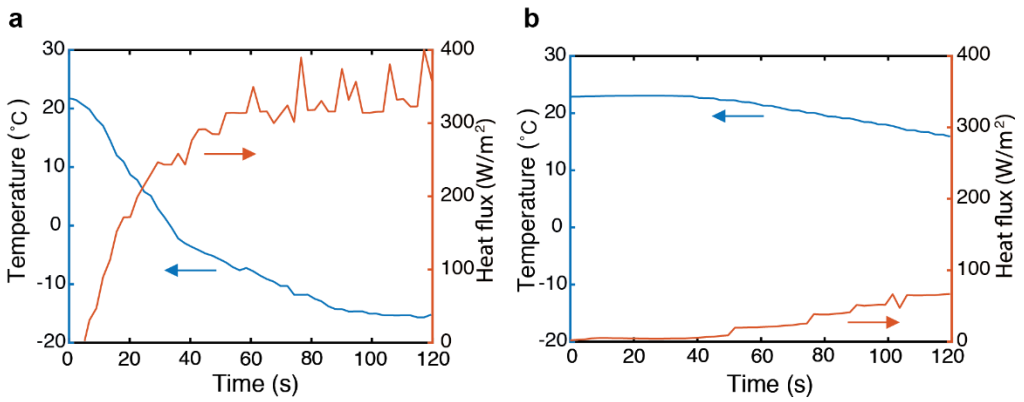

Figure S10. **Transient thermal insulation test.** Transient temperature and heat flux at the center of the top surface after the insulation material is placed on the low-temperature metal plate, for foam insulation (**a**) and the damaged VIA (**b**).

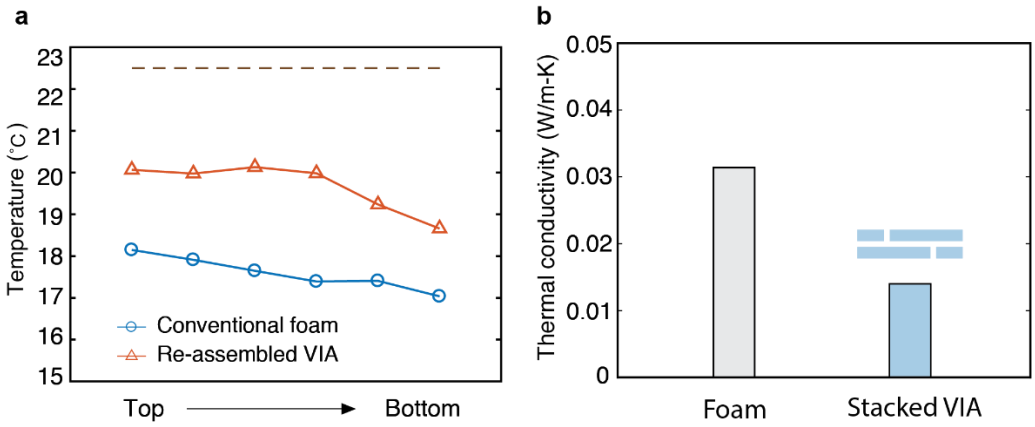

Figure S11. **Thermal insulation performance of re-assembled VIA. a**, Average temperature from the top to the bottom extracted from the infrared images shown in Figs. 3j-k. The temperature is averaged in an area of $1 \times 10\ \mathrm{cm}^2$ centered along the vertical centerline. The environment temperature is indicated by the dashed line ($22.5\ ^\circ\mathrm{C}$). **b**, Comparison of effective thermal conductivity over a given area for different insulation materials measured using the guarded hot plate method. The area is indicated by the white dashed line in Figs. 3j-k.

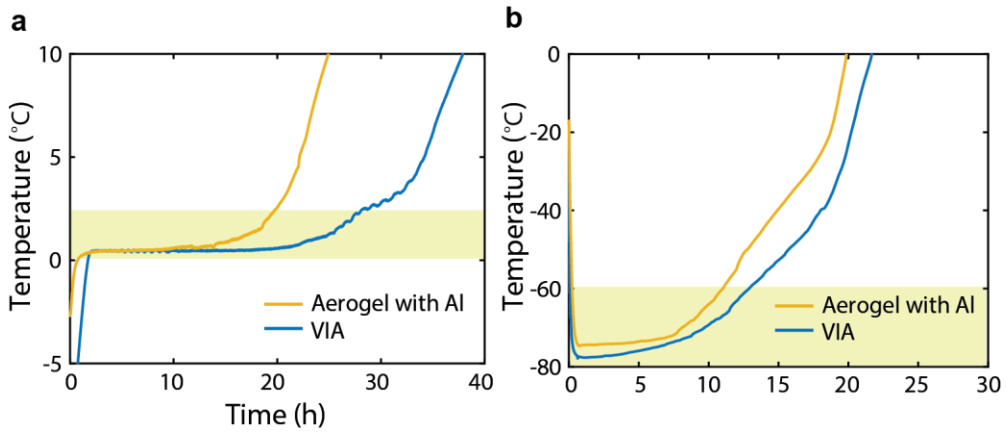

Figure S12. **Cold storage test comparing VIA and aerogel-composite insulation**. **a**, Inside-box temperature variation using ice as the phase change material. **b**, Temperature variation using dry ice as the phase change material.

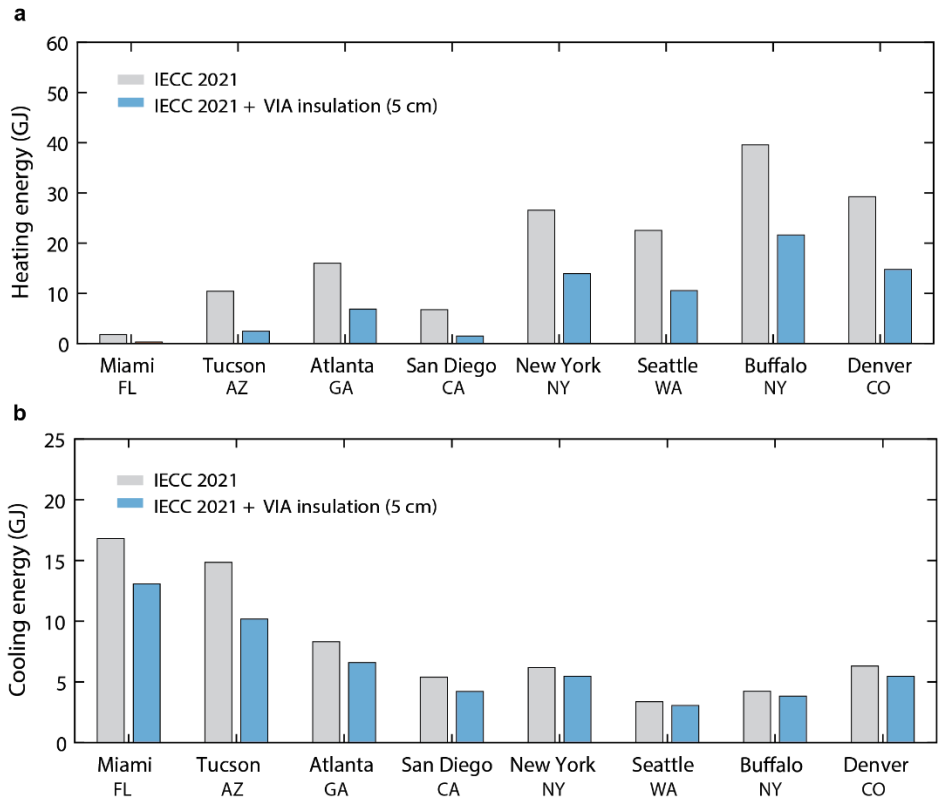

Figure S13. **Energy saving analysis with thicker insulation layer**. Annual heating energy consumption (**a**) and annual cooling energy consumption (**b**) for a single-family house across the United States. Here, a 5 cm thick insulation layer with a thermal conductivity of 0.007 W/m-K is added to each heat transfer surface of the house, achieving total heating energy reduction by about 50% - 80%, and total cooling energy reduction by about 10% - 30%.